Received: 29 July 2021 | Revised: 18 October 2021 | Accepted: 8 November 2021

DOI: 10.1096/fj.202101213R

THE FASEB JOURNAL

RESEARCH ARTICLE

Cytosolic GPR37, but not GPR37L1, multimerization and its reversal by Parkin: A live cell imaging study

Tianyi Li[1] | **Sho Oasa**[1] | **Francisco Ciruela**[2] | **Lars Terenius**[1] | **Vladana Vukojević**[1] | **Per Svenningsson**[1]

[1]Department of Clinical Neuroscience, Karolinska Institutet, Stockholm, Sweden

[2]Pharmacology Unit, Department of Pathology and Experimental Therapeutics, School of Medicine and Health Sciences, Institute of Neurosciences, IDIBELL, University of Barcelona, L'Hospitalet de Llobregat, Spain

Correspondence
Tianyi Li and Per Svenningsson, Department of Clinical Neuroscience, Karolinska Institutet, NKS, Bioclinicum, J5:20 Neuro Svenningsson, 171 77 Stockholm, Sweden.
Email: tianyi.li@ki.se and per.svenningsson@ki.se

Funding information
Swedish Foundation for Strategic Research; European Research Council, Grant/Award Number: 649116; Strategic Research Program in Neuroscience

Abstract

Biochemical data have shown aggregated G protein-coupled receptor 37 (GPR37) in the cytoplasm and Lewy bodies in Parkinson's disease (PD). Properly folded GPR37 at the plasma membrane appears to be neuroprotective. GPR37, and its homologue GPR37L1, are orphan G protein-coupled receptors and their homo- and hetero-dimers have not been established. We therefore examined GPR37 and GPR37L1 dimerization and extended studies of multimerization of GPR37 to live cells. In this study, we investigated GPR37 and GPR37L1 dimerization and multimerization in live cells using three quantitative imaging methods: Fluorescence Cross-Correlation Spectroscopy, Förster Resonance Energy Transfer, and Fluorescence Lifetime Imaging Microscopy. Our data show that GPR37 and GPR37L1 form homo- and heterodimers in live N2a cells. Importantly, aggregation of GPR37, but not GPR37L1, was identified in the cytoplasm, which could be counteracted by Parkin overexpression. These data provide further evidence that GPR37 participate in cytosolic aggregation processes implicated in PD pathology.

KEYWORDS

aggregation, dimerization, G protein-coupled receptors, Pael-R, Parkinson disease

1 | INTRODUCTION

G Protein-coupled receptors (GPCRs) and their homo- and heterodimers control several physiological processes and are important drug targets in disease.[1,2] While it was long thought that GPCRs function as monomers and their oligomerization was regarded to be pathological, it is now well accepted that oligomeric GPCR complexes modify, for better or worse, the function of GPCRs. For example, pathologic GPCR oligomerization has been identified

Abbreviations: apFRET, acceptor photobleaching Förster Resonance Energy Transfer; CLSM, Confocal Laser Scanning Microscopy; Cyto, cytoplasm; E_{app}, apparent FRET efficiency; FBS, Fetal Bovine Serum; FCCS, Fluorescence Cross-Correlation Spectroscopy; FCS, Fluorescence Correlation Spectroscopy; FLIM, Fluorescence Lifetime Imaging Microscopy; GPCRs, G protein-coupled receptors; GPR37, G-protein-coupled receptor 37, also called Pael-R; GPR37L1, G-protein coupled receptor 37-like 1; Lck, plasma membrane targeting sequence; mC, mCerulean; Mem, plasma membrane; mV, mVenus; Pael-R, Parkin-associated endothelin receptor-like receptor, also called GPR37; PD, Parkinson's disease; RCCA, relative cross-correlation amplitude; tACC, temporal autocorrelation curves; tCCC, temporal cross-correlation curves; UPR, unfolded protein response.

This is an open access article under the terms of the Creative Commons Attribution-NonCommercial License, which permits use, distribution and reproduction in any medium, provided the original work is properly cited and is not used for commercial purposes.
© 2021 The Authors. *The FASEB Journal* published by Wiley Periodicals LLC on behalf of Federation of American Societies for Experimental Biology.

for the angiotensin II AT1 receptor, which was shown to contribute to atherosclerosis and Alzheimer's disease,[3–5] whereas rhodopsin, a classical GPCR, has been shown to be functionally active as a dimer[6] and misfolded and aggregated rhodopsin was identified in retinal disease.[7]

The rhodopsin-like GPCR, G protein-coupled receptor 37 (GPR37), also called Parkin-associated endothelin receptor-like receptor (Pael-R), is a substrate of parkin E3 ubiquitin ligase.[8] GPR37 has been reported to be one of the components constituting the core structure of Lewy bodies.[8,9] Based on this, and other corroborating findings, it was suggested that misfolded and aggregated GPR37 might be involved in early pathological events in Parkinson's disease (PD).[10] Furthermore, it was shown that aggregated GPR37 induces cells death *via* ER stress.[8] Accordingly, transgenic or viral-mediated overexpression of GPR37 induced protein aggregation and dopaminergic neurons death in animal models.[11,12] However, we have found a protective role of GPR37 against dopaminergic toxins, including MPP+, rotenone and 6-OHDA, when GPR37 is properly folded and trafficked to the plasma membrane in N2a neuroblastoma cells.[13] Thus, folding, aggregation and cellular localization of GPR37 define its role in neurodegenerative *versus* neuroprotective processes.

Thus far, evidence for GPR37 misfolding and aggregation come nearly exclusively from biochemical studies, showing the formation of high-molecular-mass GPR37 aggregates by sodium dodecyl sulphate–polyacrylamide gel electrophoresis (SDS-PAGE), and immunocytochemistry, which shows intracellular GPR37 accumulation in fixed cells.[8] Given the disruptive nature of biochemical studies and the important dynamics of GPR37 intracellular trafficking, we used here several advanced fluorescence microscopy-based methods including Fluorescence Cross-Correlation Spectroscopy (FCCS), Förster Resonance Energy Transfer (FRET) and Fluorescence Lifetime Imaging Microscopy (FLIM), to examine GPR37 multimerization in live cells. In parallel, we assessed the GPR37 homologue GPR37L1 that bears 68% similarity and 48% identity with GPR37.[14] Like GPR37, GPR37L1 is an orphan GPCR that is almost exclusively expressed in the central nervous system (CNS). However, while both receptors show some homology, they have important differences: (i) GPR37L1 has a much shorter N-terminal ectodomain (109 aa) than GPR37 (N-terminal ectodomain: 239aa), which mainly leads to their different amino acid lengths and molecular weights (GPR37: 613aa, 67.12 kDa versus GPR37L1: 481aa, 52.81 kDa); (ii) GPR37L1 and GPR37 differ in their propensities to bind dopamine 2 receptors[15]; and (iii) whereas GPR37 has been implicated in Parkinsonism, GPR37L1 is implicated in cerebellar development[16] and seizure susceptibility in a novel type of progressive myoclonus epilepsy.[17]

2 | MATERIAL AND METHODS

2.1 | Plasmid construction

Human GPR37 and GPR37L1 were amplified and subcloned into pmiRFP670-N1, mVenus-N1 and mCerulean-N1. A plasma membrane targeting sequence, Lck (MGCVCSSNPE) was constructed by primers. Phusion High-Fidelity DNA Polymerase (Thermo Fisher Scientific, Waltham, MA, USA) was used in all polymerase chain reactions (PCR). Restriction endonucleases (XhoI and EcoRI) and T4 ligase were purchased from New England Biolabs (NEB; Ipswich, MA, USA). The primers used are available in Table S1. The plasmids C5V, C32V (in which Cerulean is attached to Venus with either a 5 or a 32 amino acids long linker), mVenus-N1 and mCerulean-N1 were obtained from Steven S. Vogel[18] (Addgene plasmid #26394, 26396, 27793, 27795). pmiRFP670-N1 was obtained from Vladislav Verkhusha[19] (Addgene plasmid #79987). mCherry-Parkin was a kind gift from Richard Youle[20] (Addgene plasmid #23956, #47560).

2.2 | Cell culture and transfection

N2a mouse neuroblastoma cells, obtained from ATCC (CCL-131™ Mus musculus brain neuroblastoma), were maintained in Dulbecco's Modified Eagle's Medium (DMEM) supplemented with high glucose, 10% Fetal Bovine Serum (FBS), 1% penicillin/streptomycin (final concentration 100 U/ml of penicillin and 100 μg/ml of streptomycin), 10 mM HEPES, 1 mM sodium pyruvate, 2 mM L-GlutaMAX and 1 × Non-Essential Amino Acids (NEAA) (all from Thermo Fisher Scientific, Waltham, MA, USA).

For transient expression, wild type N2a cells were seeded in 8-well chambered coverglass (Nunc Lab-Tek #155411 or Nunc Lab-Tek #155409, Thermo Fisher Scientific, Waltham, MA, USA) at a density of 1.5×10^4 cells per well. Transfections were performed by adding 80 ng of GPR37 and/or GPR37L1 encoding plasmids using 1 μl Lipofectamine 2000 (Thermo Fisher Scientific, Waltham, MA, USA) per well. Transiently expressed N2a cells were subjected to FCCS, FRET and FLIM measurements at 18–24 h after transfection.

2.3 | Live cell imaging

Confocal Laser Scanning Microscopy (CLSM) imaging of live cells expressing GPR37 and/or GPR37L1 genetically fused with eGFP or RFP670 was performed using the Zeiss Airyscan 880 inverted microscope system equipped with an Ar-ion laser (with three lines: 458, 488, and 514 nm) and a 633 nm He-Ne laser, a Plan Apochromat

40×/1.4 oil immersion objective, main dichroic beam splitter 488/561/633, emission filters BP 493–598 nm (eGFP) and BP 638–747 nm (RFP670), and a GaAsP PMT detector. To minimalize signal cross-talk, the multitrack acquisition mode was used. Image post-processing was not applied, except for brightness and contrast adjustment applied to the image, using the ZEN 2 software (Carl Zeiss, Oberkochen, Germany).

2.4 | Acceptor photobleaching FRET (apFRET)

Intensity-based FRET, i.e., acceptor photobleaching FRET method (apFRET) measurements were performed using the LSM 880 Airyscan microscope and the mCerulean (FRET donor) and mVenus (FRET acceptor) labeled receptors in live cells.[21] To begin with, fluorescence was excited using the 458 nm line of the Ar-ion laser and collected in the ranges: 463–498 nm (mCerulean) and 517–579 nm (mVenus), and five images of the selected cell were acquired by recording donor fluorescence in the presence of the acceptor. Thereafter, the acceptor was irreversibly photobleached, either in the plasma membrane or in the whole cell (GPR37-mC and -mV co-expressed with mCherry-parkin), using the 514 nm line of the Ar-ion laser at 100% transmission. Acceptor photobleaching conditions were optimized to ensure that more than 50% of the initial mVenus fluorescence intensity was lost, while ascertaining that the donor was not also bleached. Following acceptor photobleaching, time series of donor and acceptor fluorescence were acquired at 1 s intervals for 30 s, using exactly the same optical setting as before acceptor photobleaching. Changes in fluorescence intensity over time in selected regions of interest (ROIs), at the plasma membrane or in the cytoplasm, were analyzed.

The apparent FRET efficiency, E_{app} (%) was calculated as follows[21]:

$$E_{app}(\%) = \frac{I_{mC,post} - I_{mC,pre}}{I_{mC,post}} \times 100 \quad (1)$$

In Equation (1), $I_{mC,pre}$ and $I_{mC,post}$ are the background subtracted fluorescence intensities of the mCerulean (the FRET donor) before and after acceptor photobleaching, respectively. To verify the increase of mCerulean intensity upon acceptor photobleaching and in order to minimize any possible artifacts, e.g., due to reversible acceptor photobleaching, Pearson product moment correlation coefficient "*r*" between fluorescent intensities of mCerulean (donor) and mVenus (acceptor), was calculated from the apFRET experiments. Experiments for which the "*r*" values were between −0.7 and −1.0, were regarded to be artifact-free and corresponding to FRET efficiency values >3%.[22] "*r*" values were between −0.74 and −1.0 in our data except the negative control ($r = -0.23 \pm 0.62$).

2.5 | Fluorescence cross-correlation spectroscopy (FCCS)

FCCS measurements, briefly summarized in Figure S1, were performed using the individually modified LSM510 ConfoCor3 system (Carl Zeiss, Oberkochen, Germany)[23] equipped with an Ar-ion (458, 477, 488 and 514 nm), 633 nm HeNe laser, C-Apochromat 40×/1.2 water immersion UV-VIS-IR objective and Avalanche Photodiode (SPCM-AQR-1X, PerkinElmer, Waltham, MA, USA) detectors. eGFP was excited using the 488 nm line of the Ar-ion laser and RFP670 using the HeNe 633 nm laser. The main dichroic beam splitter 488/543/633 was used to separate the incident and elastically scattered light from emitted fluorescence; band pass filter BP 505–530 and long pass filter LP655 were used to further spectrally narrow eGFP and RFP670 fluorescence, respectively. The 488/633 in vitro Standard Probe for FCCS (IBA Lifesciences, Göttingen, Germany) was used for instrument alignment (Figure S1E,F). Pinhole positioning was further confirmed by measuring eGFP and RFP670 fluorescence in the culture medium.

To find the apical membrane, fluorescence intensity along the vertical axis was recorded, so-called *z*-scan (Figure S1A,B). Fluorescence intensity fluctuations were recorded in arrays of 5–10 consecutive measurements, each measurement lasting 10–15 s (Figure S1C).

FCCS data were analyzed by temporal autocorrelation using the online FCS data analysis package that is part of the running software and the ZEN 2 software (Carl Zeiss, Oberkochen, Germany). The temporal autocorrelation curves (tACC; $G_i(\tau) = f(\tau)$; Figure S1D green and magenta) and temporal cross-correlation curves (tCCC, $G_c(\tau) = f(\tau)$; Figure S1D black) were analyzed by fitting analytical equations for two-component diffusion (Equations (2) and (3)), to derive the average number of receptor molecules, and the numb of receptor-receptor dimers.

$$G_i(\tau) = 1 + \frac{1}{N_i} \cdot \left[1 + \frac{T_i}{1 - T_i} e^{-\frac{\tau}{\tau_{T,i}}}\right] \cdot \left(\sum_{l=1}^{2} \frac{f_{Di,l}}{\left(1 + \frac{\tau}{\tau_{D_{i,l}}}\right)\sqrt{1 + \frac{1}{S_i^2} \cdot \frac{\tau}{\tau_{D_{i,l}}}}} \right) \quad (2)$$

$$G_c(\tau) = 1 + \frac{N_{GR}}{N_G \cdot N_R} \cdot \left(\sum_{l=1}^{2} \frac{f_{D_{c,l}}}{\left(1 + \frac{\tau}{\tau_{D_{c,l}}}\right)\sqrt{1 + \frac{1}{Sc^2} \cdot \frac{\tau}{\tau_{D_{c,l}}}}} \right) \quad (3)$$

where, i = Green or Red channel, N_i is the average number of molecules in the corresponding observation volume element, T and τ_T are the average fraction of fluorescent molecules in the triplet state and the corresponding triplet correlation time, respectively, $\tau_{Di,l}$ is the diffusion time of fraction $l = 1$ and $l = 2$ in the ith channel, $f_{Di,l}$ is the relative fractional percentage of each diffusional component, s is the structural parameter ($s = \omega_z/\omega_{xy}$) in which ω_{xy} and ω_z are the lateral and axial $1/e$ radius of the observation volume element; and N_{GR} is the average number of dually labeled molecules. Values of the radius ω_{xy} and ω_z were determined in calibration measurements using Rh6G, $D_{\text{Rh6G}} = 4.14 \times 10^{-6}$ cm^2/s[24,25] or Cy5 ($D_{\text{Cy5}} = 3.6 \times 10^{-6}$ cm^2/s).[26]

To assess the extent of binding between receptors tagged with eGFP and RFP670, the relative cross-correlation amplitude (RCCA) was computed:

$$\text{RCCA} = \frac{A_C}{A_G}, \tag{4}$$

where A_G is the amplitude of the tACC in the green annel, $A_G = G(\tau) - 1$ at lag time $\tau = 0$ μs (Equation (2)); A_C is the amplitude of the tCCC, $A_C = G_C(\tau) - 1$ at lag time $\tau = 0$ μs (Equation (3)).

2.6 | Fluorescence Lifetime Imaging Microscopy (FLIM)

FLIM was performed using our home-built scanning-free confocal fluorescence microscope for massively parallel Fluorescence Correlation Spectroscopy (mpFCS).[27,28] In the mpFCS system, a Diffractive Optical Element (DOE) is used to create, from a single 482 nm pulsed laser beam, a rectangular illumination matrix of 16 × 16 (256) point sources (Figure S2A), that is optically conjugated with a 2D single-photon avalanche diode (SPAD) arrays camera (spc^3 single photo counting camera, Micro Photon Devices MPD, Italy) and fluorescence signals from the 256 independent points are simultaneously detected. Fluorescence lifetime, τ_f, was measured using the time-gated mode, 2 ns gate and 0.2 ns gate shift during 20 ns. To achieve a better signal to noise ratio, FLIM data was collected for 10 min.

Fluorescence lifetime, τ_f, was determined by fitting a single-exponential decay function to the FLIM decay curve (Figure S2B):

$$I(t) = Ae^{-\frac{t-t_{\text{offset}}}{\tau_f}} + I_{\text{B}} \tag{5}$$

In Equation (5), $I(t)$ is the photon counts at time t, A is the amplitude of the FLIM curve, t_{offset} is offset time of FLIM curve corresponding to the pulse arrival time during the FLIM time window, and I_B is the background photon counts.

2.7 | Nanoluciferase Binary Technology (NanoBiT) assay

cDNA encoding the human GPR37 and D2R (long splice variant) were cloned into pIREShyg3 plasmid vector (Clontech Laboratories, Inc.) containing the sequences for either the small (SmBiT) or long (LgBiT) subunit of the nanoluciferase,[29] respectively. N2a cells were transfected with appropriate combinations of plasmids (1 μg/well of each plasmid) using 8 μl Lipofectamine 2000 (Thermo Fisher Scientific, Waltham, MA, USA) in a 6-well plate. After 20–24 h, transfected N2a cells (4×10^4 cells/well) were seeded in a complete growth medium onto a 96-well plate (Corning, New York, USA) previously coated with 10 μg/ml poly-D-lysine. The next day, the medium was removed from each well and replaced with 90 μl Opti-MEM (Thermo Fisher Scientific, Waltham, MA, USA) before 10 μl of a 10 μM coelenterazine 400a solution (NanoLight Technologies, Pinetop, AZ, USA) was added to each well. Then the plate was incubated for 10 min in the dark at 37 °C, allowing reaction to occur. Luciferase signal was detected with a Tecan Spark 10M microplate reader (Männedorf, Switzerland) and the output luminescence reported as the integrated relative light units (RLU).

2.8 | Data and statistical analysis

All data are presented as mean ± standard deviation (SD). Numbers of cells analyzed in each graph are given in the corresponding figure legend. Two-tailed Student's t-test was used to compare two groups. Kruskal-Wallis test followed by Dunn's post hoc correction was used to compare the multiple groups in RCCA. Brown-Forsythe and Welch ANOVA test followed by Dunnett's T3 post hoc correction was used to compare FRET efficiencies and also differences (Δ) in the fluorescence lifetime among groups. Multiple paired t test followed by holm-šídák correction was used to compare fluorescence lifetime. All statistical analyses were performed using GraphPad Prism 9 (San Diego, CA, USA). Differences were considered to be significant when $p < .05$.

3 | RESULTS

3.1 | Fluorescence cross-correlation spectroscopy (FCCS) shows that the propensities of GPR37 and GPR37L1 to form homo- and heteromers in the plasma membrane of live N2a cells are similar

CLSM imaging shows GPR37/GPR37L1 co-localization in the cytoplasm and plasma membrane of live N2a cells transiently expressing receptors fluorescently tagged by genetic fusion with eGFP or RFP670 (Figure 1A). Comparing to eGFP tag,[15] the RFP670 tag is not changing the diffusion properties of GPR37 (Figure S3). FCCS shows that GPR37 and GPR37L1 form both homo- and heteromers in the plasma membrane (Figure 1B,C). The relative cross-correlation amplitude (RCCA), which is a proxy for the degree of binding—the higher the RCCA the higher the binding (Equation (3)), was similar ($p > .05$) for all three variants tested: GPR37 homomer (0.21 ± 0.11), GPR37L1 homomer (0.21 ± 0.09) and GPR37-GPR37L1 (0.23 ± 0.12) heteromer, (Figure 1C). Given the similar expression levels of GPR37 and GPR37L1 (Figure S4), this suggests that the binding degrees for GPR37 and GPR37L1 homo- and heteromers are similar.

While CLSM imaging showed that GPR37/GPR37L1 co-localize also in the cytoplasm (Figure 1A), it was not possible to characterize by FCCS their degree of binding in the cytoplasm due to extensive photobleaching. In addition, FCCS cannot assess the extent of GPR37/GPR37L1 homo- and heteromerization in the immobile fraction of GPR37/GPR37L1 receptors in the plasma membrane—GPR37 receptors are organized in the plasma membrane into distinct micro-domains, which may partly restrict their lateral movements.[30] Finally, FCCS confirms co-migration of GPR37/GPR37L1 homo- and heteromers, but cannot distinguish whether the receptor molecules are directly bound to one another, forming homo- and heterodimers, or form larger molecular assemblies with one or more other proteins. To answer these questions, Förster Resonance Energy Transfer (FRET) *via* acceptor photobleaching (apFRET) was used as it can provide complementary insights about receptor-receptor binding at the nanoscale (1–10 nm). To this aim, mCerulean- and mVenus-tagged GPR37/GPR37L1 receptors were used. GPR37/GPR37L1 homo- and heteromerization was further characterized by monitoring eGFP fluorescence lifetime in cells expressing eGFP-tagged GPR37/GPR37L1 receptors. In addition, GPR37-GPR37 interactions in live cells were found using the NanoBiT assay (Figure S5).

3.2 | Acceptor photobleaching FRET (apFRET) shows that the propensities of GPR37 and GPR37L1 to form homo- and heterodimers in the plasma membrane of live N2a cells are similar

In line with the data shown in Figure 1A, CLSM imaging showed that mCerulean- and mVenus-tagged GPR37 and GPR37L1 receptors co-localize in the plasma membrane and in the cytoplasm (Figures 2A and S6). Quantification of signal intensity following apFRET assay, showed a significant increase in mCerulean intensity after mVenus bleaching, confirming that a nonradiative transfer of energy has occurred from excited mCerulean to mVenus. This, in turn, indicates that the donor and the acceptor molecules are in close proximity, i.e., at distances 1–10 nm, which is indicative of homo- and heterodimer formation. Apparent FRET efficiency, E_{app}, which reflects the percentage of energy transferred from the donor fluorophore to the acceptor fluorophore (Equation (1)), showed that FRET efficiency in all cases was significantly higher than negative control (Figure 2B), confirming GPR37 and GPR37L1 homo- and heterodimerization in the plasma membrane. Importantly, FRET efficiency was similar for all variants tested: heterodimer GPR37-GPR37L1 (E_{app} = (15 ± 7) %) and homodimers GPR37-GPR37 (E_{app} = (14 ± 6) %) and GPR37L1-GPR37L1 (E_{app} = (13 ± 5) %) (Figure 2B). However, this difference was not statistically significant ($p > .05$), suggesting that the propensities of GPR37 and GPR37L1 to form homo- and heterodimers are similar.

Given that intensity-based FRET methods, such as apFRET are susceptible to variations due to, for example, differences in protein expression levels in different cells, extent of acceptor photobleaching, extent of unwanted donor photobleaching, molecular diffusion, we have resorted to fluorescence lifetime imaging that is not affected by factors such as excitation source intensity, light absorption/scattering in the sample or fluorophore photobleaching.

3.3 | Fluorescence lifetime imaging microscopy (FLIM) suggests that GPR37 and GPR37L1 differ in their propensity to aggregate in the membranous matrix of the cytoplasm of live N2a cells

Scanning-free massively parallel FLIM system[27,28] was used to map eGFP fluorescence lifetime, $\tau_{f,eGFP}$, in live N2a cells expressing eGFP-tagged GPR37 or GPR37L1 (Figure 3A,B). Interestingly, FLIM showed that in N2a cells expressing GPR37-eGFP, eGFP fluorescence

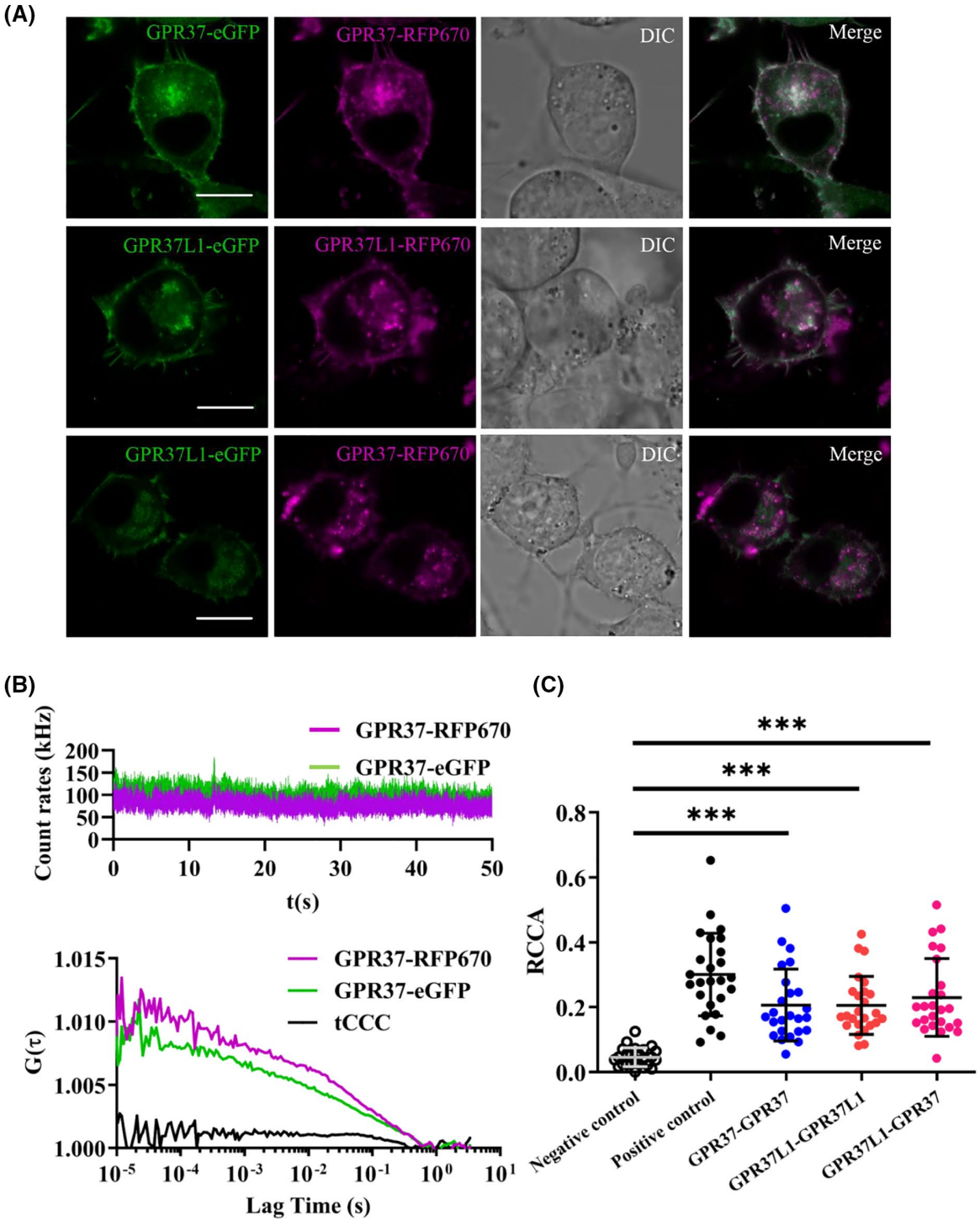

FIGURE 1 Fluorescence Cross-Correlation Spectroscopy (FCCS) shows that fluorescently tagged GPR37 and GPR37L1 receptors form homo- and heteromers in the plasma membrane of live N2a cells. (A) CLSM images showing GPR37-eGFP and GPR37-RFP670 (top); GPR37L1-eGFP and GPR37L1-RFP670 (middle); GPR37-eGFP and GPR37L1-RFP670 (bottom) co-localization in the cytoplasm and the plasma membrane (scale bar: 10 μm). (B) *Top*: eGFP (green) and RFP670 (magenta) fluorescence intensity fluctuations over time recorded in the plasma membrane. *Bottom*: Corresponding temporal auto- (green and magenta) and cross-correlation (black) curves. (C) Relative cross-correlation amplitudes (RCCA). *Negative control*: N2a cells co-expressing eGFP and RFP670; *Positive control*: N2a cells expressing cell membrane protein Lck labelled with the eGFP-RP670 fusion protein (Lck-eGFP-RP670); GPR37–GPR37: N2a cells co-expressing GPR37-eGFP and GPR37-RFP670; GPR37L1–GPR37L1: N2a cells co-expressing GPR37L1-eGFP and GPR37L1-RFP670; GPR37L1–GPR37: N2a cells co-expressing GPR37L1-eGFP and GPR37-RFP670. The RCCA values are given as mean ± SD ($n = 25$). ***$p < .001$, significantly different from eGFP–RFP670 as negative control. Kruskal-Wallis test followed by Dunn's post hoc correction

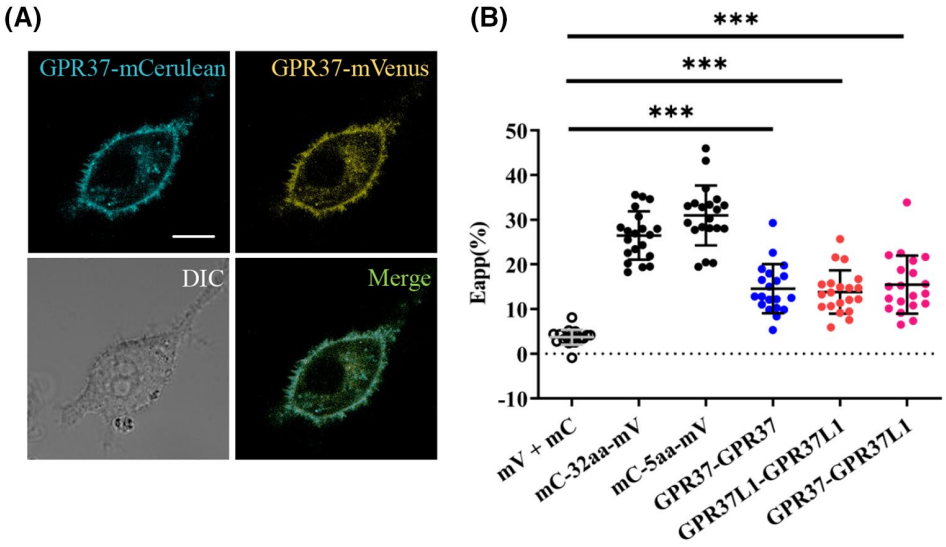

FIGURE 2 Fluorescence resonance energy transfer (FRET) identifies homo- and heterodimerization of GPR37 and GPR37L1 in the plasma membrane of live N2a cells. (A) CLSM images showing GPR37-mVenus and GPR37-mCerulean co-localization in the cytoplasm and the plasma membrane (scale bar: 10 μm). (B) FRET efficiency. *Negative control*: N2a cells co-expressing empty-mCerulean-N1 and empty-mVenus-N1 plasmids (mV + mC); *Positive control*: mCerulean-32aa-mVenus and mCerulean-5aa-mVenus fusion protein with long and short linker respectively; GPR37–GPR37: N2a cells co-expressing GPR37-mCerulean and GPR37-mVenus; GPR37L1–GPR37L1: N2a cells co-expressing GPR37L1-mCerulean and GPR37L1-mVenus; GPR37L1–GPR37: N2a cells co-expressing GPR37-mCerulean and GPR37L1-mVenus. FRET efficiencies, as determined using apFRET ($n = 20$), are shown as (mean ± SD). ***$p < .001$, significantly different from negative control, mV + mC. Brown-Forsythe and Welch ANOVA test followed by Dunnett's T3 post hoc correction

lifetime in the plasma membrane was significantly longer than in the cytoplasm (Figure 3C), in contrast to cells expressing GPR37L1-eGFP, where eGFP fluorescence lifetime was similar in both compartments (Figure 3D).

While fluorescence lifetime depends on the local micro-environment immediately surrounding the fluorophore, such as local pH, viscosity, oxygen concentration, an increased singlet to ground state radiative transition probability was previously observed upon aggregation when eGFP was fused to an aggregation-prone peptide, which revealed itself through a decrease in eGFP fluorescence lifetime.[31]

3.4 | Parkin overexpression counteracts GPR37-eGFP aggregation using FLIM and apFRET measurements

In order to determine whether the measured reduction in eGFP fluorescence lifetime may be caused by GPR37-eGFP self-assembly in the cytoplasm, we co-expressed Parkin, an E3-Ubiqutin ligase that recognizes unfolded GPR37 as a substrate and promotes its degradation.[8] We hypothesized that if GPR37-eGFP aggregates in the cytoplasm and Parkin can prevent aggregation *via* the degradation of unfolded GPR37, eGFP fluorescence lifetime should increase upon Parkin co-expression. Indeed, we have observed that fluorescence lifetime of GPR37-eGFP in the cytoplasm became significantly longer in cells co-expressing Parkin (Figure 3E), in line with the expected reduction in GPR37-eGFP aggregation. In contrast, eGFP fluorescence lifetime in the cytoplasm of cells expressing GPR37L1-eGFP was insensitive to Parkin coexpression (Figure 3F). We further characterized the effect of Parkin on GPR37-GPR37 interaction by apFRET using mCerulean (mC)-/mVenus (mV)-labeled GPR37. We have observed that in the presence of Parkin the apparent FRET efficiency of GPR37-mC and GPR37-mV was significantly lower than without Parkin (Figure 3G), consistent with our hypothesis that in the presence of Parkin GPR37 shows less propensity to aggregate. In addition, CLSM imaging showed that GPR37 and GPR37L1 mainly localize in membranous structures in the cytoplasm, presumably the Golgi apparatus, as revealed by colocalization with Golgi markers Golgi-3-mPlum and Giantin-mScarlet (Figure S7). However, only GPR37 aggregates in this subcellular compartment.

A protective role of GPR37 against dopaminergic toxins (MPP+, rotenone and 6-OHDA) has been found when GPR37 is properly folded and trafficked to the plasma membrane in N2a neuroblastoma cells.[13] We therefore tested whether the subcellular localizations of GPR37 or GPR37L1 changes during a short (2 h) cell exposure to dopaminergic toxins by assessing whether

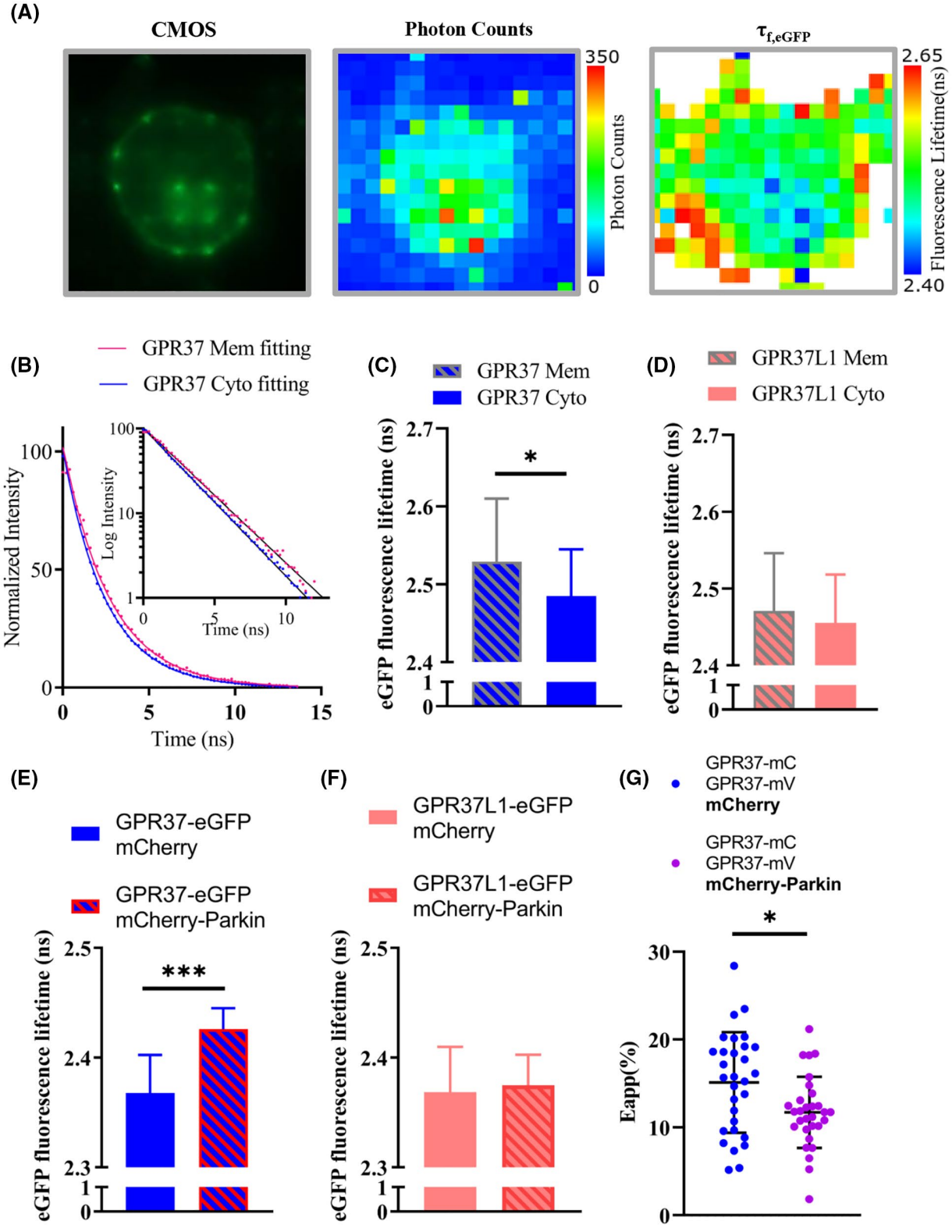

the ratio of membrane- and cytoplasm-associated fluorescence (F_m/F_c) changes over time. However, we have found that under these experimental conditions, the F_m/F_c ratio remains at a similar level for both GPR37 and GPR37L1 in the absence or presence of MPP+ or 6-OHDA (Figure S8).

4 | DISCUSSION

In our study, GPR37-GPR37, GPR37L1-GPR37L1 and GPR37-GPR37L1 interactions were examined in live cells. We have observed that GPR37 and GPR37L1 form homo- and heterodimers in the plasma membrane, and

FIGURE 3 Fluorescence lifetime imaging microscopy (FLIM) identifies GPR37 aggregates formation in the cytoplasm of live N2a cells. (A) Images of a typical N2a cell expressing GPR37-eGFP. *Left*: Fluorescence intensity image acquired using spot wise illumination and a Canon 20 megapixel digital single-lens reflex (DSLR) camera. *Middle*: Fluorescence intensity image acquired using spot-wise illumination and an SPC3 single-photon counting camera by MPD. *Right*: Fluorescence lifetime image. (B) Fluorescence decay curves of eGFP in the plasma membrane (Mem) and the cytoplasm (Cyto) of live N2a cells expressing GPR37-eGFP. *Inset*: Logarithmic plot of the fluorescence decay curves. Solid lines are derived by fitting single-exponential functions to the experimentally derived curves (symbols). (C,D) eGFP fluorescence lifetime in the cytoplasm (Cyto) and the plasma membrane (Mem). The results shown are mean ± SD, $n = 17$. *$p < .05$, ***$p < .001$. Multiple paired *t* test followed by holm-šídák correction. (E,F) aggregates of GPR37-eGFP in the cytoplasm was attenuated by mCherry-Parkin as reflected by fluorescence lifetime increment. Unpaired *t* test with Welch's correction for GPR37 ($n = 20$), ***$p < .001$; fluorescence lifetime increment was not observed in the cells co-expressing GPR37-eGFP and mCherry-Parkin. Unpaired *t* test for GPR37L1 ($n = 11$). (G) Parkin attenuated interaction of GPR37-mC and GPR37-mV as reflected by lower FRET efficiency. $n = 30$, Unpaired *t* test, *$p < .05$

have characterized GPR37 aggregation in the cytoplasm by FLIM.

Physiological functions of GPR37 and GPR37L1 are not fully elucidated. To our knowledge, the X-ray crystallography or cryogenic electron microscopy (cryo-EM) structures of GPR37 and GPR37L1 have not been revealed. However, all class A GPCRs share a structural topology characterized by seven transmembrane (TM) helices at the plasma membrane. Sequence analysis revealed that GPR37 and GPR37L1 are homologous. Alignment of GPR37 and GPR37L1 shows sequence conservation in the TM regions and the presence of a cysteine cluster at the C-terminal end (Figure S9). Although they have different length of their N-terminal ectodomains, both are subject to metalloprotease-dependent proteolytic N-terminus processing. Both GPR37 and GPR37L1 N-terminal peptides have been found in cerebrospinal fluid (CSF).[32–34] Interestingly, peptides from the ectodomain of GPR37 are increased in CSF from PD patients.[33] Under normal physiological conditions, GPR37 folds in the ER, passes to the Golgi apparatus and is delivered to the plasma membrane. Misfolded GPR37 is sent to the proteasome for degradation. During pathological processes, the balance between GPR37 being properly folded or misfolded, and subsequently degraded, is disturbed by various factors causing accumulation of the misfolded protein, ER stress and the activation of the unfolded protein response (UPR).[10] There are a few studies on GPR37/GPR37L1 interacting with D2R and A2A receptors.[15,35,36] However, homo- and heterodimerization of GPR37 and GPR37L1 are unclear especially in different cellular compartments in live cells.

As GPCR dimers and/or oligomers at the plasma membrane have emerged as a possible mechanism for lateral organization and GPCR lateral diffusion has been an important factor in membrane protein interaction, FCCS is an ideal tool to examine GPCR-GPCR interaction as reflected by their co-migration at the plasma membrane. However, as for all methods, there are limitations. A limitation of FCCS is the bleed through giving rise to a false cross-correlation between channels. In our study, by using a recently developed monomeric near-fared RFP with emission at 670 nm,[19] the bleed through has been largely limited. Nevertheless, a cross-correlation was still observed indicating that the cross-correlation detected is not due to cross-talk between fluorescent channels. Another limitation is that only mobile GPCRs at the plasma membrane can be detected by FCCS. However, lateral movement of GPCRs have been reported to be restricted by membrane structure or cell skeleton.[37] Therefore, we need another technique to include immobile GPCRs at the plasma membrane in our assessment. As a complementary method, FRET, which is independent of the mobility of molecules, was used in our study. Besides, direct interaction without participation of other proteins can be addressed as distance of energy transfer is shorter than 10 nm.[38]

GPR37 aggregation has been implicated in the pathogenesis of Parkinson's disease.[10] However, as we mentioned above, all reported evidences for existence of GPR37 aggregation come from biochemical studies. Fluorescence lifetime imaging enables us to extend the previous work and to evaluate protein aggregation in live cells. In order to compare fluorescence lifetimes in the plasma membrane and intracellular regions, spatial mapping of fluorescence lifetime in real time was achieved by scanning-free confocal imaging *via* massively parallel FCS integrated with FLIM (mpFCS/FLIM), which enabled us to simultaneously obtain fluorescence lifetime data from different subcellular regions. By comparing to the fluorescence lifetime of eGFP at the plasma membrane and in the cytoplasm, we could see that eGFP fluorescence lifetime is shorter in the later. This has prompted us to examine whether co-expression of Parkin alters eGFP fluorescence lifetime in the cytoplasm, as shortened eGFP fluorescence lifetime in the cytoplasm may be due to GPR37-eGFP aggregation. Parkin, namely mediates transfer of ubiquitin from E2 to unfolded and aggregated GPR37 to prevent them from causing UPR-induced cell death.[8,39] Indeed, eGFP fluorescence lifetime in the cytoplasm increased when Parkin was co-expressed with GPR37-eGFP, suggesting

that this ubiquitin ligase counteracts GPR37 multimerization. In contrast, cytoplasmic eGFP fluorescence lifetime of GPR37L1 was insensitive to Parkin co-expression.

At the plasma membrane, GPR37L1-eGFP showed a shorter fluorescence lifetime comparing to GPR37-eGFP which may be due to differences in the membranous microenvironment where the receptors express themselves. However, this needs to be further studied since homodimers of GPR37 and GPR37L1 at the plasma membrane showed similar interactions using FCCS and FRET.

5 | CONCLUSIONS

Using advanced biophysical approaches we have provided evidence that GPR37 and GPR37L1 form homo- and heterodimers in the plasma membrane of live N2a cells; we have shown that the propensities of GPR37 and GPR37L1 to form homo- and heterodimers in the plasma membrane of live N2a cells are similar, and that GPR37, but not GPR37L1, aggregates in the cytoplasm. Moreover, our data corroborate previous findings that Parkin is an important regulator of GPR37 aggregation and is effective in preventing the accumulation of GPR37 aggregates in the cytoplasm of live cells.

ACKNOWLEDGMENTS

This study was financially supported by the Swedish Foundation for Strategic Research and European Research Council (Progsy). Financial support by the Strategic Research Program in Neuroscience (StratNeuro) to SO is gratefully acknowledged.

DISCLOSURES

The authors declared no conflict of interest.

AUTHOR CONTRIBUTIONS

Tianyi Li, Vladana Vukojević, Lars Terenius, and Per Svenningsson conceived and designed the research. Francisco Ciruela provided reagents. Data were generated by Tianyi Li, with Sho Oasa overseeing the FLIM experiments. Data were analyzed by Tianyi Li Data were interpreted by all authors. Tianyi Li created the figures. All authors were involved in the writing.

ORCID

Tianyi Li https://orcid.org/0000-0002-7161-0987
Sho Oasa https://orcid.org/0000-0003-3800-590X
Francisco Ciruela https://orcid.org/0000-0003-0832-3739
Lars Terenius https://orcid.org/0000-0003-2880-9576
Vladana Vukojević https://orcid.org/0000-0003-0873-5653
Per Svenningsson https://orcid.org/0000-0001-6727-3802

REFERENCES

1. Lohse MJ. Dimerization in GPCR mobility and signaling. *Curr Opin Pharmacol*. 2010;10:53-58.
2. Wang W, Qiao Y, Li Z. New insights into modes of GPCR activation. *Trends Pharmacol Sci*. 2018;39:367-386.
3. AbdAlla S, Lother H, Langer A, el Faramawy Y, Quitterer U. Factor XIIIA transglutaminase crosslinks AT1 receptor dimers of monocytes at the onset of atherosclerosis. *Cell*. 2004;119:343-354.
4. AbdAlla S, Lother H, el Missiry A, et al. Dominant negative AT2 receptor oligomers induce G-protein arrest and symptoms of neurodegeneration. *J Biol Chem*. 2009;284:6566-6574.
5. Quitterer U, AbdAlla S. Discovery of pathologic GPCR aggregation. *Front Med*. 2019;6:9.
6. Liang Y, Fotiadis D, Filipek S, Saperstein DA, Palczewski K, Engel A. Organization of the G protein-coupled receptors rhodopsin and opsin in native membranes. *J Biol Chem*. 2003;278:21655-21662.
7. Park PSH. Rhodopsin oligomerization and aggregation. *J Membrane Biol*. 2019;252:413-423.
8. Imai Y, Soda M, Inoue H, Hattori N, Mizuno Y, Takahashi R. An unfolded putative transmembrane polypeptide, which can lead to endoplasmic reticulum stress, is a substrate of Parkin. *Cell*. 2001;105:891-902.
9. Murakami T, Shoji M, Imai Y, et al. Pael-R is accumulated in Lewy bodies of Parkinson's disease. *Ann Neurol*. 2004;55:439-442.
10. Leinartaité L, Svenningsson P. Folding underlies bidirectional role of GPR37/Pael-R in Parkinson disease. *Trends Pharmacol Sci*. 2017;38:749-760.
11. Kitao Y, Imai Y, Ozawa K, et al. Pael receptor induces death of dopaminergic neurons in the substantia nigra via endoplasmic reticulum stress and dopamine toxicity, which is enhanced under condition of parkin inactivation. *Hum Mol Genet*. 2007;16:50-60.
12. Dusonchet J, Bensadoun JC, Schneider BL, Aebischer P. Targeted overexpression of the parkin substrate Pael-R in the nigrostriatal system of adult rats to model Parkinson's disease. *Neurobiol Dis*. 2009;35:32-41.
13. Lundius EG, Stroth N, Vukojević V, Terenius L, Svenningsson P. Functional GPR37 trafficking protects against toxicity induced by 6-OHDA, MPP+ or rotenone in a catecholaminergic cell line. *J Neurochem*. 2013;124:410-417.
14. Smith NJ. Drug discovery opportunities at the endothelin B receptor-related orphan G protein-coupled receptors, GPR37 and GPR37L1. *Front Pharmacol*. 2015;6:e00275.
15. Hertz E, Terenius L, Vukojević V, Svenningsson P. GPR37 and GPR37L1 differently interact with dopamine 2 receptors in live cells. *Neuropharmacology*. 2019;152:51-57.
16. Marazziti D, Di Pietro C, Golini E, et al. Precocious cerebellum development and improved motor functions in mice lacking the astrocyte cilium-, patched 1-associated Gpr37l1 receptor. *Proc Natl Acad Sci USA*. 2013;110:16486-16491.

17. Giddens MM, Wong JC, Schroeder JP, et al. GPR37L1 modulates seizure susceptibility: evidence from mouse studies and analyses of a human GPR37L1 variant. *Neurobiol Dis*. 2017;106:181-190.
18. Koushik SV, Chen H, Thaler C, Puhl HL 3rd, Vogel SS. Cerulean, venus, and VenusY67C FRET reference standards. *Biophys J*. 2006;91:L99-L101.
19. Shcherbakova DM, Baloban M, Emelyanov AV, Brenowitz M, Guo P, Verkhusha VV. Bright monomeric near-infrared fluorescent proteins as tags and biosensors for multiscale imaging. *Nat Commun*. 2016;7:12405.
20. Narendra D, Tanaka A, Suen DF, Youle RJ. Parkin is recruited selectively to impaired mitochondria and promotes their autophagy. *J Cell Biol*. 2008;183:795-803.
21. Broussard JA, Rappaz B, Webb DJ, Brown CM. Fluorescence resonance energy transfer microscopy as demonstrated by measuring the activation of the serine/threonine kinase Akt. *Nat Protoc*. 2013;8:265-281.
22. Bu W, Lim KB, Yu YH, Chou AM, Sudhaharan T, Ahmed S. Cdc42 interaction with N-WASP and Toca-1 regulates membrane tubulation, vesicle formation and vesicle motility: implications for endocytosis. *PLoS One*. 2010;5:e12153.
23. Vukojevic V, Heidkamp M, Ming Y, Johansson B, Terenius L, Rigler R. Quantitative single-molecule imaging by confocal laser scanning microscopy. *Proc Natl Acad Sci USA*. 2008;105:18176-18181.
24. Petrásek Z, Schwille P. Precise measurement of diffusion coefficients using scanning fluorescence correlation spectroscopy. *Biophys J*. 2008;94:1437-1448.
25. Muller CB, Loman A, Pacheco V, et al. Precise measurement of diffusion by multi-color dual-focus fluorescence correlation spectroscopy. *Epl-Europhys Lett*. 2008;83(4):46001.
26. Loman A, Müller CB, Koberling F, Richtering W, Enderlein J. Absolute and precise measurements of the diffusion of small fluorescent dye molecules across the visible spectrum. Poster, 14th International Workshop on Single Molecule Spectroscopy and Ultrasensitive Analysis in Life Sciences; 2008.
27. Krmpot AJ, Nikolić SN, Oasa S, et al. Functional fluorescence microscopy imaging: quantitative scanning-free confocal fluorescence microscopy for the characterization of fast dynamic processes in live cells. *Anal Chem*. 2019;91:11129-11137.
28. Vitali M, Bronzi D, Krmpot AJ, et al. A single-photon avalanche camera for fluorescence lifetime imaging microscopy and correlation spectroscopy. *IEEE J Sel Top Quant*. 2014;20:344-353.
29. Wouters E, Vasudevan L, Ciruela F, Saini DK, Stove C, Van Craenenbroeck K. Assessing GPCR dimerization in living cells: comparison of the NanoBiT assay with related bioluminescence- and fluorescence-based approaches. In: Fuxe K, Borroto-Escuela DO, eds. *Receptor-Receptor Interactions in the Central Nervous System*. Springer; 2018:239-250.
30. Lundius EG, Vukojevic V, Hertz E, et al. GPR37 protein trafficking to the plasma membrane regulated by prosaposin and GM1 gangliosides promotes cell viability. *J Biol Chem*. 2014;289:4660-4673.
31. Ghukasyan V, Hsu CC, Liu CR, Kao FJ, Cheng TH. Fluorescence lifetime dynamics of enhanced green fluorescent protein in protein aggregates with expanded polyglutamine. *J Biomed Optics*. 2010;15:016008.
32. Coleman JLJ, Ngo T, Smythe RE, et al. The N-terminus of GPR37L1 is proteolytically processed by matrix metalloproteases. *Sci Rep*. 2020;10:19995.
33. Mattila SO, Tuusa JT, Petaja-Repo UE. The Parkinson's-disease-associated receptor GPR37 undergoes metalloproteinase-mediated N-terminal cleavage and ectodomain shedding. *J Cell Sci*. 2016;129:1366-1377.
34. Morato X, Garcia-Esparcia P, Argerich J, et al. Ecto-GPR37: a potential biomarker for Parkinson's disease. *Transl Neurodegener*. 2021;10:8.
35. Dunham JH, Meyer RC, Garcia EL, Hall RA. GPR37 surface expression enhancement via N-terminal truncation or protein-protein interactions. *Biochemistry*. 2009;48:10286-10297.
36. Morató X, Luján R, López-Cano M, et al. The Parkinson's disease-associated GPR37 receptor interacts with striatal adenosine A(2A) receptor controlling its cell surface expression and function in vivo. *Sci Rep*. 2017;7:9452.
37. Jacobson K, Liu P, Lagerholm BC. The lateral organization and mobility of plasma membrane components. *Cell*. 2019;177:806-819.
38. Vogel SS, van der Meer BW, Blank PS. Estimating the distance separating fluorescent protein FRET pairs. *Methods*. 2014;66:131-138.
39. Wang HQ, Imai Y, Inoue H, et al. Pael-R transgenic mice crossed with parkin deficient mice displayed progressive and selective catecholaminergic neuronal loss. *J Neurochem*. 2008;107:171-185.

SUPPORTING INFORMATION

Additional supporting information may be found in the online version of the article at the publisher's website.

How to cite this article: Li T, Oasa S, Ciruela F, Terenius L, Vukojević V, Svenningsson P. Cytosolic GPR37, but not GPR37L1, multimerization and its reversal by Parkin: A live cell imaging study. *FASEB J*. 2021;35:e22055. doi:10.1096/fj.202101213R